Astron. Nachr. / AN **328**, No. 8, 743 – 746 (2007) / **DOI** 10.1002/asna.200710795

Numerical simulations of fast and slow coronal mass ejections

T. Török[1,⋆] and **B. Kliem**[2,3]

[1] University College London, Mullard Space Science Laboratory, Holmbury St. Mary, Dorking, Surrey, RH5 6NT, U.K.
[2] Astrophysical Institute Potsdam, An der Sternwarte 16, D-14482 Potsdam, Germany
[3] Kiepenheuer-Institut für Sonnenphysik, Schöneckstraße 6, D-79104 Freiburg, Germany

Received 2007 Mar 26, accepted 2007 May 24
Published online 2007 Sep 19

Key words Sun: corona – Sun: coronal mass ejections (CMEs) – Sun: filaments – Sun: flares – Sun: magnetic fields

Solar coronal mass ejections (CMEs) show a large variety in their kinematic properties. CMEs originating in active regions and accompanied by strong flares are usually faster and accelerated more impulsively than CMEs associated with filament eruptions outside active regions and weak flares. It has been proposed more than two decades ago that there are two separate types of CMEs, fast (impulsive) CMEs and slow (gradual) CMEs. However, this concept may not be valid, since the large data sets acquired in recent years do not show two distinct peaks in the CME velocity distribution and reveal that both fast and slow CMEs can be accompanied by both weak and strong flares. We present numerical simulations which confirm our earlier analytical result that a flux-rope CME model permits describing fast and slow CMEs in a unified manner. We consider a force-free coronal magnetic flux rope embedded in the potential field of model bipolar and quadrupolar active regions. The eruption is driven by the torus instability which occurs if the field overlying the flux rope decreases sufficiently rapidly with height. The acceleration profile depends on the steepness of this field decrease, corresponding to fast CMEs for rapid decrease, as is typical of active regions, and to slow CMEs for gentle decrease, as is typical of the quiet Sun. Complex (quadrupolar) active regions lead to the fastest CMEs.

1 Introduction

Coronal mass ejections (CMEs) are spontaneous ejections of plasma and magnetic flux from the inner solar corona into interplanetary space. They can originate in active regions, where they are associated with X-ray or EUV flares and often also with filament eruptions, but they can also originate from eruptions of large quiescent filaments outside active regions not accompanied by strong flares. Early observations, based on relatively small data sets, indicated that flare-related CMEs are faster, often moving already at nearly constant speed (mostly in excess of ≈ 750 km s^{-1}) when they enter the field of view of white-light coronagraphs, i.e., they are fully accelerated at heliocentric distances $< 2R_\odot$, whereas CMEs with weak or no flare activity are accelerated only gradually to moderate speeds (typically $\approx$ 400–600 km s^{-1}) within the coronagraph field of view of 6 $R_\odot$ or more.

Such data led MacQueen & Fisher (1983) to suggest the existence of two separate types of CMEs, flare-associated ones and eruption-associated ones (Fig. 1), the latter referring to quiescent filament eruptions. Their concept has been supported by Sheeley et al. (1999), who categorised the two types as impulsive and gradual, respectively. Both author groups suggested that the acceleration is dominated by different physical processes, which may imply the need for different models.

⋆ Corresponding author: e-mail: tt@mssl.ucl.ac.uk

Studies of the large CME data sets meanwhile available revealed a very wide range of kinematic properties, with velocities ranging from ~ 50 – 3000 km s^{-1} and accelerations ranging from ~ 10 to $> 10^4$ m s^{-2} over $\sim$ 5–1000 minutes. However, the data always showed a continuous distribution of velocities with a single peak (Zhang & Dere 2006 and references therein). Furthermore, both fast and slow CMEs can be accompanied by both weak and strong flares (Vršnak, Sudar & Ruždjak 2005). These findings suggest that the concept of physically different CME types might not be valid, rather there may exist a continuous distribution of CME kinematics, with fast impulsive and slow gradual CMEs representing the two ends of the distribution.

Theoretical models of CMEs did not address the wide range of CME kinematics for many years. Some modellers reproduced the trajectories of individual filament eruptions and CMEs in good agreement with the observations (e.g., Krall et al. 2001; Chen & Krall 2003; Török & Kliem 2004, 2005; Williams et al. 2005; Chen et al. 2006). A first attempt to model impulsive and gradual CMEs in a unified manner was presented by Chen & Krall (2003). These authors enforced the expansion of a line-tied, semi-toroidal flux rope by driving it out of equilibrium through the "injection" of poloidal magnetic flux at the photospheric level. The acceleration of the rope is dominated by its Lorentz self-force (hoop force) and significant only during the period of flux injection. A range of acceleration profiles of the rope apex, encompassing impulsive and gradual CMEs, was obtained

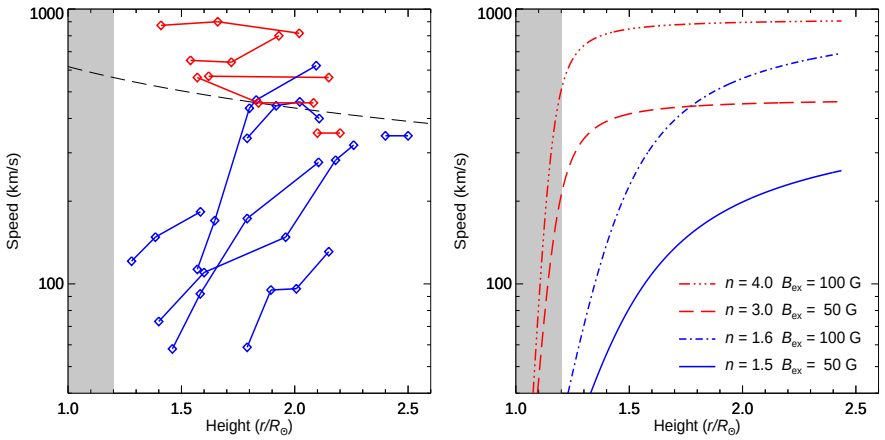

Fig. 1 *Left:* observation of two apparently distinct CME types (data from MacQueen & Fisher 1983): fast CMEs (red) acquire nearly constant speeds low in the corona (behind the coronagraph's occulting disk indicated in grey), while slow CMEs (blue) are accelerated only gradually to reach the gravitational escape speed (dashed line). *Right:* the TI of a freely expanding current ring yields similar velocity profiles for different decay indices n of the external poloidal field $B_{\rm ex}$ (equilibrium field strengths at the initial radius $R_0 = 10$ Mm are given).

by prescribing different amplidudes and durations of the injection and by varying geometrical parameters of the rope.

Recently, we suggested a flux rope model which explains the wide range of CME kinematics without the need of such external driving (Kliem & Török 2006, hereafter KT06). As in the model of Chen & Krall (2003), the flux rope expands due to the hoop force, but the eruption is caused by an ideal MHD instability, the torus instability (TI). A range of flux rope trajectories encompassing impulsive and gradual events results naturally from the model if the height dependence of the magnetic field overlying the flux rope is varied. However, the analytical treatment of CME acceleration in KT06 required simplifications, notably a freely expanding circular current ring (rather than a line-tied flux rope) was considered, and flux pileup, pressure gradients, and external toroidal fields had to be neglected.

In this paper, we present MHD simulations of the TI which include the effects of photospheric line tying and of flux pileup in front of the expanding rope. By considering a substantial range of magnetic field profiles above the flux rope, we confirm our previous result (KT06) that the TI of a flux rope provides a CME model which describes both impulsive and gradual CMEs and their association with the main magnetic structural properties of their source region.

2 Torus instability

Observations of erupting filaments, which often evolve into the cores of CMEs, suggest the magnetic topology of a single arched magnetic flux rope, or partial current ring, whose footpoints are anchored in the solar surface. As is well known from fusion research, the required pre-eruption equilibrium in a low-beta environment must include an external poloidal magnetic field $\boldsymbol{B}_{\rm ex}$, since the hoop force, as well as the net pressure gradient force, of a bent non-neutralized current channel always point radially outward. Such a current ring is unstable against expansion if its hoop force decreases more slowly with major ring radius R than the opposing Lorentz force due to $B_{\rm ex}$ (Bateman 1978). Assuming $B_{\rm ex} \propto R^{-n}$, where $n = -R\,d\ln B_{\rm ex}/dR$ is the decay index of the external field, Bateman (1978) found $n > n_{\rm cr} = 3/2$ as condition for the instability.

KT06 suggested the instability as a possible initiation and driving mechanism for CMEs, referring to it as torus instability, and treated its evolution for the first time (using the same external field as Bateman 1978). It was found that the acceleration profile of the freely expanding current ring strongly depends on the steepness of the external field decrease with R. For moderate to steep decrease, $n \gtrsim 2$, the acceleration rises quickly to a peak within $R/R_0 \lesssim 2$ and decreases quickly afterwards, resulting in a profile as observed in impulsive CMEs. The peak acceleration increases, and its radial position decreases, with increasing n, so that the CME develops a more impulsive trajectory if it originates in more localized and more complex flux concentrations. For very gradual decrease (n approaching n_{cr}), the acceleration has a gradual profile, nearly uniformly distributed over a large radial range, i.e., with small peak value shifted to larger R; see Fig. 1 in KT06.

Hence, the instability produces not only a continuum of acceleration profiles ranging from fast impulsive to slow gradual ones, it also reproduces the observed association of impulsive profiles with highly concentrated flux in the source (active regions, high n) and of gradual profiles with the gradual field decrease over a large height range in the quiet Sun ($n \sim 3/2$, Vršnak et al. 2002). Fig. 1 shows a comparison of velocity profiles obtained from this model with observed CME velocities. We note that more gradual profiles result also if R_0 is increased (which compresses the x axis of the right panel in Fig. 1 proportionally); this is the effect used by Chen & Krall (2003). Both small n and large R_0 make large-scale quiescent filament eruptions gradual.

3 Numerical simulations

In order to confirm the analytical results, we perform 3D zero-beta ideal MHD simulations of the TI, using the approximately force-free coronal flux rope model by Titov & Démoulin (1999) as initial condition. The line-tied flux rope corresponds to a current ring partly submerged in the dense subphotospheric plasma.

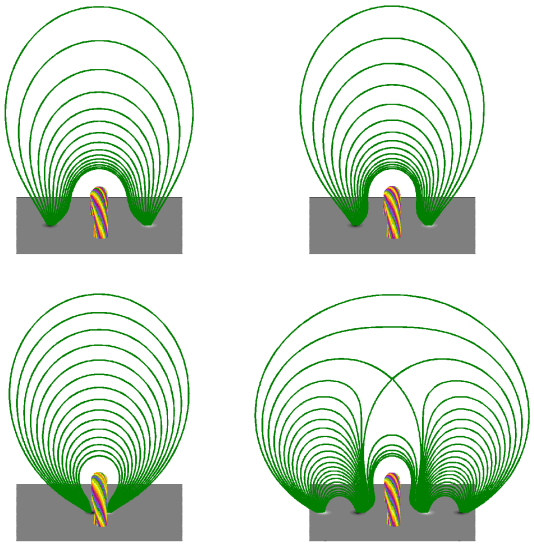

Fig. 2 Initial configurations of the numerical simulations, corresponding to the red, blue, green, and black lines in Figure 3, respectively (from top left to bottom right). The rainbow-coloured field lines show the centre of the flux rope (current ring), the green field lines show the overlying magnetic field (which is a superposition of the external poloidal field B_{ex} and the poloidal field created by the ring current). Normalized distances between the monopoles are 3.6, 2.7, and $0.5\,h_0$ in the bipolar configurations and 2.5 and $5.0\,h_0$ in the quadrupolar one.

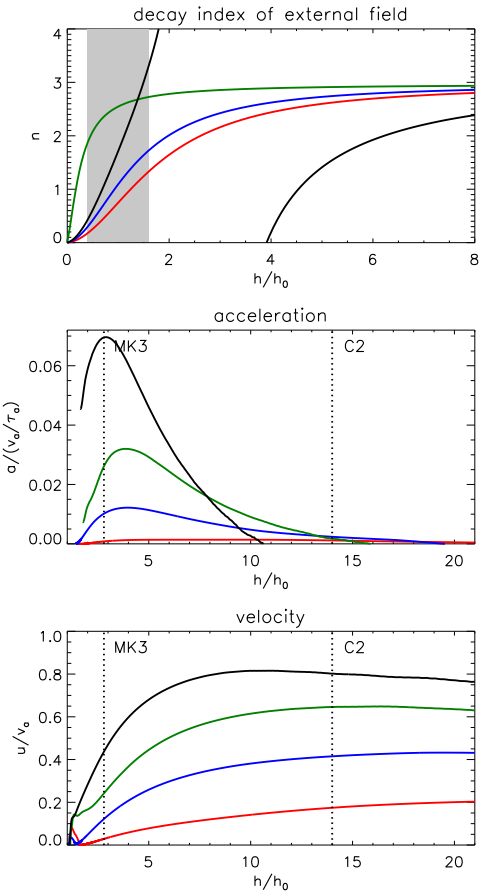

Fig. 3 Decay indices $n(h) = -h\,d\ln B_{\rm ex}/dh$ of the external poloidal field and corresponding acceleration and velocity profiles for the torus-unstable flux ropes shown in Fig. 2 ($|n| \to \infty$ at the null in the quadrupolar configuration). The initial position of the current-carrying flux rope is indicated in grey. The inner edges of the MK3 and LASCO/C2 coronagraph fields of view are indicated for a scaled initial apex height of the flux rope of 50 Mm. Velocities are normalized to the initial Alfvén velocity v_a at the flux rope apex; $\tau_a = h_0/v_a$. The acceleration during the initial relaxation phase is omitted for clarity of the figure.

The setup and initial conditions of the simulations are similar to those described in Török & Kliem (2005). Here we use a flux rope with a smaller aspect ratio by setting its minor radius to $6/10$ of its initial apex height h_0 (to obtain a configuration with a flux rope twist below the threshold of the helical kink instability) and we choose the initial flux rope shape to be almost semi-circular by setting the depth of the torus center below the photosphere to be only $0.1\,h_0$ (since the line-tying suppresses the TI before a semi-circular shape is reached; Vršnak, Ruždjak & Rompolt 1991; Chen et al. 2006). Furthermore, we remove the toroidal component of the external field used in Török & Kliem (2005), to facilitate the comparison with the analytical TI model. The resulting purely poloidal external field is created by a pair of subphotospheric monopoles (see Titov & Démoulin 1999). It is more realistic than the one used in KT06, as it yields a decay index which increases monotonically with height above the photosphere, $n = n(h)$.

We fix the geometrical flux rope parameters and consider different external field profiles by varying the number, position and strength of the subphotospheric monopoles in the model (such that the variations of the ring current and the flux rope twist stay below 1%). The resulting configurations are shown in Fig. 2. The field above the flux rope of the configuration in the bottom right panel is quadrupolar and contains an X-line. The top panel in Fig. 3 shows the corresponding decay indices $n(h)$ of the external fields. The external field in the quadrupolar configuration drops very rapidly with height, with $n(h) > 3$ already in the region immediately above the rope. The other configurations all have external fields with $n(h) < 3$ above the rope, but with different slopes. As $h \to \infty$, $n \to 3$ for all configurations.

The TI is found to occur also in the numerical model. It is triggered by moderate upward motions set up in the initial relaxation phase of the only approximatively force-free configuration, which lift the flux rope to a height where the conditions for TI onset ($2h_0 \gtrsim D$, D being the footpoint distance, and $n(h) > n_{\rm cr}$) are fulfilled. In the case shown in the top left panel in Fig. 2, the field decrease is so gradual that the initial relaxation does not move the flux rope to the height required for TI onset, the rope finds a stable numerical equilibrium after relaxation. In order to trigger the TI in this configuration, we artificially set the monopole strength to be 9% smaller than its equilibrium value, which causes the rope to relax towards an equilibrium at a slightly greater height, sufficient for TI onset. The simulations show agree-

ment with the analytically obtained instability threshold: in the two runs with the lowest $n(h)$ profile, the TI starts at flux rope apex heights where $n \lesssim 1.5$.

Despite the differences between the analytical and the numerical model, the rise profiles are qualitatively very similar (compare Fig. 3 with Fig. 1 in KT06). In both cases, the acceleration rises quickly to a maximum which strongly increases with the steepness of the external field decrease. Afterwards, the steeper the field decrease, the steeper the drop of the acceleration. In the numerical model, the peak acceleration is shifted to somewhat greater heights for fast ejections, $h/h_0 \sim 2$–4, which appears to conform better to the observations than the analytical result ($h/h_0 \approx 2$).

The quadrupolar configuration yields the most impulsive acceleration and the highest terminal velocity.

4 Conclusions and discussion

We present numerical simulations of an erupting force-free magnetic flux rope embedded in the potential field of model bipolar and quadrupolar active regions. The eruption is driven by the TI which occurs if the external poloidal field decreases sufficiently rapidly with height. The simulations show that the TI occurs not only in freely expanding current rings (KT06), but also in line-tied flux ropes. The TI threshold is similar in both cases, $n_{\rm cr} \sim 3/2$.

The acceleration profile depends on the steepness of the field decrease, corresponding to fast CMEs for rapid decrease (as is typical of active regions) and to slow CMEs for gradual decrease (as is typical of the quiet Sun). These simulations confirm our previous finding (KT06) that the TI permits to describe fast and slow CMEs in a unfied manner. This demonstrates, in accordance with the observational results in Vršnak, Sudar & Ruždjak (2005) and Zhang & Dere (2006), that the concept of two separate CME types is not valid and that the wide range of CME kinematics can be explained by a single underlying physical process.

The ratio of the maximum velocities (accelerations) in the fastest and the slowest eruption in Fig. 3 is ≈ 4 (≈ 40). These ranges are about one order of magnitude smaller than the corresponding ranges observed in CMEs. However, it is important to note that the peak velocities and accelerations listed in the Introduction are matched with very reasonable choices for the Alfvén speed in the core of large active regions ($v_a \sim 3750$ km s^{-1}) and for h_0 ($\lesssim R_\odot/10$), although the inclusion of line tying and flux pileup in front of the expanding rope in the numerical model reduce the acceleration considerably in comparison to the analytical result. The great majority of observed CME speeds and accelerations is accommodated for if the variations of v_a and h_0 between δ spots and quiescent filaments, both by factors 3–10, are taken into account. It is always possible to match extremely slow CMEs by setting the parameters of the simulation very close to the instability threshold. Moreover, for gradual CMEs which result from eruptions of quiescent filaments and are accelerated over several $R_\odot$, the presence of the heliospheric current sheet reduces the decay index of the overlying field in comparison to the asymptotic value ($n = 3$) in the Titov & Démoulin equilibrium.

Magnetic fields in multipolar active regions decrease in the lower corona faster with height than those in bipolar active regions or in the quiet Sun. Consequently, our model predicts the fastest CMEs to originate in multipolar active regions, which is in line with observations. No "breakout-like" reconnection above the flux rope is required in our simulation of the quadrupolar model configuration, the eruption is solely driven by the TI.

In contrast to the model of Chen & Krall (2003), our model allows to obtain a wide range of CME kinematics without imposing an external driving of the configuration with a duration similar to the observed duration of significant acceleration. For given flux rope parameters, the kinematics are determined by the slope of the magnetic field overlying the flux rope. Although the magnetic field in the corona cannot be measured directly at present, a wide range of height profiles of the field can be expected to exist, as the large variety of field distributions revealed by photospheric magnetograms indicates.

We note that, for a given overlying field, the acceleration profile also depends on the chosen flux rope parameters as well as on the existence of a flux rope velocity at TI onset (due to external perturbations; Schrijver et al. 2007). Furthermore, we expect that an external toroidal field and pressure gradients will influence the evolution as well. These effects will be studied in forthcoming work.

Acknowledgements. We thank the referee for constructive comments. T. T. thanks the British Council and PPARC for financial support. B. K. was supported by the DFG.

References

Bateman, G.: 1978, *MHD Instabilities*, MIT, Cambridge
Chen, J., Krall, J.: 2003, JGR 108, 1410
Chen, J., Marqué, C., Vourlidas, A., Krall, J., Schuck, P. W.: 2006, ApJ 649, 452
Kliem, B., Török, T.: 2006, PhRvL 96, 255002 (KT06)
Krall, J., Chen, J., Duffin, R. T., Howard, R. A., Thompson, B. J.: 2001, ApJ 562, 1045
MacQueen, R. M., Fisher, R. R.: 1983, SoPh 89, 89
Sheeley, N. R., Walters, J. H., Wang, Y.-M., Howard, R. A.: 1999, JGR 104, 24739
Schrijver, C. J., Elmore, C., Kliem, B., Török, T., Title, A. M.: 2007, ApJ, *in press*, arXiv:0710.1609
Titov, V. S., Démoulin, P.: 1999, A&A 351, 707
Török, T., Kliem, B.: 2004, in Proc. *SOHO 15–Coronal Heating*, eds. R. W. Walsh et al., ESA SP-575, 56
Török, T., Kliem, B.: 2005, ApJ 630, L97
Vršnak, B., Magdalenić, J., Aurass, H., Mann, G.: 2002: A&A 396, 673
Vršnak, B., Ruždjak, V., Rompolt, B.: 1991, SoPh 136, 151
Vršnak, B., Sudar, D., Ruždjak, V.: 2005, A&A 435, 1149
Williams, D. R., Török, T., Démoulin, P., van Driel-Gesztelyi, L., Kliem, B.: 2005, ApJ 628, L163
Zhang, J., Dere, K. P.: 2006, ApJ 649, 1100

